symmetry

MDPI

Article

Influence of Asymmetric Agglomerations Effects over the Photothermal Release of Liposome-Encapsulated Nanodiamonds Assisted by Opto-Mechanical Changes

Samuel Morales-Bonilla [1,*], Isaac I. Mota-Díaz [2], Janna Douda [2], Ariel Fuerte-Hernández [3], Juan Pablo Campos-López [3] and Carlos Torres-Torres [1,*]

[1] Escuela Superior de Ingeniería Mecánica y Eléctrica Unidad Zacatenco, Instituto Politécnico Nacional, Ciudad de México 07738, Mexico
[2] Unidad Profesional Interdisciplinaria en Ingeniería y Tecnologías Avanzadas, Instituto Politécnico Nacional, Ciudad de México 07320, Mexico
[3] División de Ingeniería Mecatrónica, Universidad Politécnica del Valle de México, Tultitlan 54910, Mexico
* Correspondence: smoralesbo@ipn.mx (S.M.-B.); ctorrest@ipn.mx (C.T.-T.)

Abstract: An analysis of optical effects exhibited by blood plasma under healthy/unhealthy conditions, and of the penetrating evolution of nanovehicles conformed by nanodiamonds (NDs) encapsulating liposomes (L) within these biofluids, is presented. Optical ablation of liposome clusters was actuated and controlled by a standard two-wave mixing (λ = 532 nm, τp = 4 ns) laser light method. Radiant time exposure effects (30 min) and threshold laser energy parameters (250 mJ/cm^2 numerical; 181 mJ/cm^2 experimental) necessary to release NDs were identified and confirmed with similar experiments in the literature. Interactions during the sedimentation process between nanovehicles and the laser beams barrier were considered as the principal thermal damage process to achieve the release and transportation of drugs within these static fluids. The mechanical response during the release of NDs focuses on the temperature propagation, dynamic effects of nanovehicles associated with the diffusion coefficient, and some agglomeration effects. The principal findings of this research concern the threshold temperature (51.85 °C) of liposomes for the release of NDs with respect to that typically quoted in the literature (40–70 °C) for pure liposomes. The assessment of the release of NDs focuses on the numerical magnitude of Quantum Yield. Furthermore, the optical contrast enhancement was associated with NDs size agglomerations and the healthy/unhealthy conditions of fluids. This research aims to be a first proof approximation for delivery and transportation approaches to guide and interpret outcomes when combined with the vectorial nature basis of laser light and further effects once the cargo is retained in the fluids.

Keywords: nanovehicles; photophysics; optics; blood plasma; nanodiamonds; liposomes; photothermal damage

Citation: Morales-Bonilla, S.; Mota-Díaz, I.I.; Douda, J.; Fuerte-Hernández, A.; Campos-López, J.P.; Torres-Torres, C. Influence of Asymmetric Agglomerations Effects over the Photothermal Release of Liposome-Encapsulated Nanodiamonds Assisted by Opto-Mechanical Changes. *Symmetry* **2023**, *15*, 775. https://doi.org/10.3390/sym15030775

Academic Editor: Christophe Humbert

Received: 28 February 2023
Revised: 13 March 2023
Accepted: 21 March 2023
Published: 22 March 2023

1. Introduction

During recent years, there has been rising importance of using nanomaterials in living systems to analyze organized structures that display specific functions. This emerging field involves the behavior of nanoparticles (NPs) that exhibit controllable small dimensions comparable to sizes of proteins (5–50 nm), viruses (20–450 nm), cells (10–100 μm), or genes (2–100 nm) [1]. These nanomaterials can act as a damage agent or a platform for therapy [2]. The therapeutic performance that can be achieved by NPs can be controlled by electromagnetic fields; thus, it is necessary to investigate the frequency of their oscillations due to the strength of the field [3]. The contrast emissions by the oscillations stop once the material has reached a stable condition, but, by pushing them out of balance, NPs will emit again. These electromagnetic reactions, combined with the intrinsic penetrability, open interesting biological applications.

Electromagnetic contrast-enhanced behavior of NPs had been already observed in biological applications including thermally induced biochemical and morphological effects in biofluids [4,5]. Some findings suggest that as blood is exposed to heat by laser irradiation, partial fragmentation of cells occurs due to physical–chemical reactions, resulting in the disintegration of proteins, and these changes generate small increments of scattering and absorption at specific wavelengths [6]. By diffusing NPs into the base fluids, the optical and mechanical properties are changed, which has brought about promising alternatives in new applications as warming and cooling nanofluids. Within these effects are implicit absorption and adsorption phenomena in cells [7]. Some of these studies have been developed to induce physical and chemical changes using light devices to raise the temperature of biological solutions and produce controlled damage via measurements of optical properties. Specifically, some researchers propose the use of Neodymium-Yttrium Garnet (Nd:YAG) laser irradiation to induce temperature changes between 60 °C and 70 °C, concluding that the cooling effect concerns (1) the purification of hemoglobin, which produces an increment in absorption and (2) denaturation, which increases the scattering which influences the transmittance response. Other researchers have investigated the requirements of short laser pulse irradiation on similar biological fluids. Those findings concluded that changes in the transmittance and reflection of pulsed dye laser light were attributed to temperature-dependent effects and the absorption properties [8]. Finally, Holmium:YAG laser pulses have demonstrated coagulation in albumen using fast flash photography [9]. The experiments of the authors concluded that thermal damage induced significantly higher light scattering due to coagulation.

Nanodiamonds (NDs) are a promising class of outstanding NPs which have attracted much attention for a wide variety of optical and heat applications [10]. They are part of a group of nanoscale carbon materials that includes carbon nanotubes, graphene, fullerene, carbon dots, and nanofibers. Many applications have been found in areas of bioimaging, cell imaging, solar cells, nanoelectronics devices, combat COVID-19, glucose sensors, photodynamic therapy, and gene delivery for these particles [11–14]. NDs combine good features such as the possibility of being produced on large scale using relatively inexpensive synthetic processes, their surfaces functionalization, good biocompatibility, and excellent wavelength light emission [15].

Furthermore, the targeting of drugs has been made possible with chemical adaptation and functionalization of NDs, usually by coating with biocompatible cells such as liposomes [16]. These lipid-based hybrid formulations represent a combination of biological advantages of lipids and unique architectural features of NPs [17]. This platform represents a promising alternative to designing personalized drugs with small sizes and surface functionalization to versatile delivery vehicles [18]. Moreover, liposomes have demonstrated their ability to entrap drugs [19]. This ability has made them a popular "modern system" for experimenting and modeling their influence in a wide variety of therapeutic processes [20]. However, the drug-entrapment capacity of liposomes is not bioavailable; it becomes bioavailable when they are released with the most efficient external mechanism [21]. In this sense, release effects are important to increase their use [22]. Apart from providing a link between NDs and liposomes working as nanovehicles, there are other advantageous characteristics. At first, liposomes can be constructed to entrap materials within aqueous and solid environments. Second, liposomes can enter the human organism without causing adverse reactions while entering into contact with living organisms. Finally, similar degradation of natural membranes within the body is also possible [23].

Motivated by the arguments mentioned above, in this research, the optical response of NDs encapsulated in liposomes (L + NDs) working as nanovehicles and released by laser pulses was studied. A two-wave mixing (TWM) assisted by nanosecond laser pulses coming from an Nd:YAG laser system was employed. In addition to the photothermal and dynamical processes for drugs delivery and transportation, the influence of agglomerations during drug transportation through blood plasma is discussed. The analysis of the absorption coefficient (α) is proposed as a promising parameter to be used in the diagnosis

of other diseases. Attractive advantages to combining liposomes and NDs mainly consist in the possibility to employ the remarkable properties of NDs as biomarkers dispersible in water, and then to apply NDs in the area of biomedical imaging. In addition, due to their outstanding photoluminescence effects, NDs allow their detection by means of fluorescent microscopy, as well as monitoring them by optical systems, such as spectrofluorimetry or biosensing.

Important functions of using NDs instead of some other carbon-based nanoparticles with liposomes are that NDs present low cytotoxicity and selective absorption in different cell lines, and they also promote cell proliferation coupled to their optical properties, which provides a large margin for applications in biomedicine.

2. Materials and Methods

2.1. Sample Preparation

Samples with blood plasma (BP) under healthy/unhealthy conditions were evaluated from adult patients with specific medical diagnosis. Thirty different cases of each kind of sample were considered. Samples A represent BP with glucose levels in acceptable parameters, without diabetes. Samples B belong to donors with blood glucose levels outside the normal range, with diabetes mellitus. Plasma viscosity of biofluids with diabetes is above of 1.2 mPa·s and without diabetes was below 1.2 mPa·s. Similarities of gender and age were considered as well during the sample collection. A reference fluid conformed by ethanol (Sample C) was considered to calibrate the optical and physical response during the experiment. Some basic optical parameters concerning each liquid set of samples were evaluated with help of a spectrometer USB2000 + XR1-ES (Ocean Optics, Orlando, FL, USA) and a DH-2000 optical source (Ocean Optics, Orlando, FL, USA). Every biological fluid was dispersed in quartz cuvettes (TEFIC, Mexico City, Mexico). Optical properties from 100 microliters (μL) of liquids were evaluated at room temperature. After deposition into the cuvettes, each sample was evaluated by the spectrometer. Surface morphology of L + NDs diluted in fluids was investigated using a Transmission Electron Microscope (TEM, FEI, Hillsboro, OR, USA, Titan 80-300, JEM-ARM200CF). The prepared formulations specimens were spread on a glass cover slip and photographs were taken from different perspectives. Samples were spread in Lacey copper grids for the TEM studies. NDs with sizes from 3 to 15 nm (95%) were shipped from Skyspring Nanomaterials Inc. (Houston, TX, USA). The materials employed for the preparation of the samples were soy lecithin powder (Supplier local), chloroform (Sigma-Aldrich, St. Louis, MO, USA), methanol, and PBS (Sigma-Aldrich). Soy lecithin blank liposomes and soy lecithin liposomes-ND were prepared using the bilayer lipid rehydration method previously described [24].

2.2. NDs Release

The TWM schematic experimental setup is sketched in Figure 1. Coherent irradiation of laser light (Item λ in Figure 1) was supplied by an Nd:YAG laser emitter, Continuum Model SL II-10, 532 nm wavelength, 4 nanosecond pulse intervals, 100 mJ maximum laser energy per pulse, a repetition rate from 1 to 10 Hz, and 5 mm of spot laser beam at the aperture. This principal coherent irradiation is divided by the beam splitter (BS, Newport, Irvine, CA, USA) into two waves entering in the sample, S. The probe beam comes from four mirrors (M1-4, Newport, Irvine, CA, USA), while the pump beam comes from two mirrors (M5-6, Newport, Irvine, CA, USA). Probe/pump beams pass through lenses (L, Newport, Irvine, CA, USA), which reduces the laser spot to 3 mm.

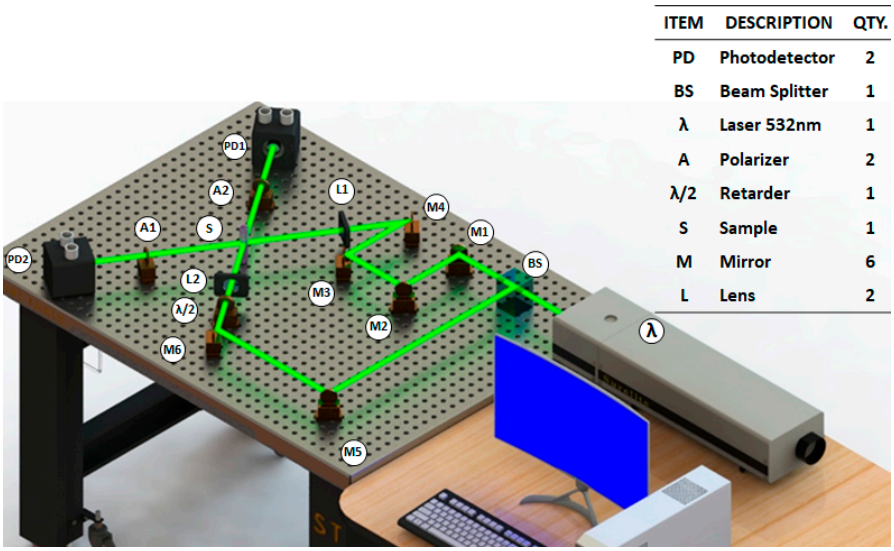

Figure 1. Experimental setup utilized for performing the laser light propagation by a TWM configuration in the samples studied.

Modulation of the irradiance provided by the superposition of probe and pump waves was controlled via a half-wave retarder ($\lambda/2$, Newport, Irvine, CA, USA). Such modulation resulted in a contrast in the wave mixing that crosses the sample. As a sample, we employed colloidal suspension of blood plasma under healthy and unhealthy conditions with nanovehicles conformed by L + NDs. The release of NDs can be produced due to ablation and/or photobleaching derived by electromagnetic irradiation of the laser system. Polarization between recording waves was analyzed via calcite polarizers (A1-2, Newport, Irvine, CA, USA). The evolution of the output laser signals was recorded using photodetectors (PD1-2, Model: 818-BB-21 Newport, Irvine, CA, USA). This experimental configuration was calibrated with CS2 (Sigma-Aldrich, St. Louis, MO, USA) in a cuvette of quartz (TEFIC, Mexico City, Mexico) and with a thickness of 1 mm to guarantee the modulation during the process of irradiance.

An important aspect related to Gaussian beams is the amount of light that passes through a medium. The incident intensity $I(\omega)$ of the light with a laser beam at a given radius, r, of which initial intensity is I_0, and an optical frequency ω, is given by [25].

$$I(\omega) = I_0 e^{-2\frac{r^2}{w^2}} \tag{1}$$

The term w represents the size of the laser beam spot and r is the spatial dimension within the media. Dimensions of w and r are in units of length (typically in mm and nm, respectively). Dimensions of $I(\omega)$ are assumed to be as arbitrary units (a.u.) because it represents the ratio of intensity of light between two points of different amplitudes and with different populations.

A laser beam focusing through a medium over a distance (z) experiences a loss of light intensity, (I), characterized by the relationship of Lambert Beer:

$$\alpha = -\log \frac{I_0}{I} \tag{2}$$

Here, I_0 is the beam intensity of the laser source. The absorption coefficient, α, is a characteristic function of the wavelength and material.

Let us consider the laser pulse energy E_P in (mJ/cm^2) and the cross-sectional area of the laser beam, (A), in (cm^2), in which $r = w$ in (cm); then, we can obtain the multi-pulse ablation threshold $F_{\text{int}}(N)$ as [26]:

$$F_{\text{int}}(N) = \beta N \frac{E_P}{A} \tag{3}$$

where $\beta = (2/e^2)$.

The number of pulses, N, is

$$N = f_{rep} \cdot t \tag{4}$$

where f_{rep} is the repetition rate or frequency in (1/s) and t is the total time of the irradiated sample in (s).

2.3. Nanovehicles Diffusion

The diffusion coefficient (D) of a mass (m) has a kinetic in organic liquids, and some characteristics, such as heat transfer, mass transfer, viscosity, and thermal conductivity, are required for its characterization [27]:

$$D = \frac{KT}{6\pi r_p \eta} \tag{5}$$

Here, (K) is the Boltzmann constant, (T) is the temperature developed within the media, (r_p) is the average radius of particles, and (η) is the viscosity of the liquid. Due to changes in temperature, additional small energy magnitudes are expected.

The Korsmeyer–Peppas equation is one of the most applied mathematical models to explain diffusion profiles as function of time [28].

$$\frac{M_t}{M_\infty} = \kappa \cdot t \tag{6}$$

In this equation, $\frac{M_t}{M_\infty}$ represents the drug diffusion rate permeated (from 0 to 100% or 0 to 1) in a time, t. While κ (kappa) refers to the nanovehicles transportation constant (dimension of time^{-1}) which provides information of the drug formulation, and n is the dimensionless transport constant related to the evolution of the drug release and the velocity of light. This equation describes the fraction (or the rate) of liposome released in a time, t, but the time units correspond to those of the constant κ (1/s) and are therefore eliminated; this means that this parameter represents a ratio of mass that changes over time.

Let us suppose that temperature (T) is a function of a Cartesian Coordinates System (x, y, z) and time (t). The evolution of heat that induces a laser source is [26]

$$\rho C_p \frac{\partial T}{\partial t} = \nabla \cdot (k \nabla T) + (1 - R) \alpha I_0 e^{-\alpha z} \tag{7}$$

where I_0 is the external short-pulses laser irradiation (bell curve distribution); alpha (α) describes the absorption coefficient, and the reflectivity of the sample is denoted by R. We also assumed that rho (ρ), (C_p), and (k) are parameters associated with heat capacity (C_p), density (ρ), and temperature conductivity (k). All these three parameters are involved in an integrated constant depicted by gamma (γ). In this case, ∇ represents the gradient operator $(\partial/\partial x, \partial/\partial y, \partial/\partial z)$.

The experiments of synthesis and characterization were carried out in triplicate, and the design of statistical nonlinear optical experiments was designed to be carried out ten times in different samples in order to identify the magnitude far from the error bar.

3. Results and Discussion

3.1. Sample Characterization

From the TEM image plotted in Figure 2a, we observe symmetric/asymmetric liposome encapsulated NDs where the liposome size can reach diameters near 150 nm. The line arrangement delineates a self-organized liposome entrapping NDs. We also observe a liposome with a perfectly circular shape which highlights the symmetry of some nanovehicles in the mixture. It is estimated that part of the NDs is encapsulated in the lipid bilayer, although it cannot be ruled out that they remain added to the surface of the liposome, or inside it. Similar variability of the shape and size due to these auto-assembly effects had been reported during the development of this kind of formulation at the administration site [29]. The total number of particles can be determined by the individual particle size within the simulation domain concerning the internal tube space. Figure 2b represents the symmetry of a circular nanoliposome without entrapping NDs. Alterations in roughness can be easily observed between Figure 2a,b.

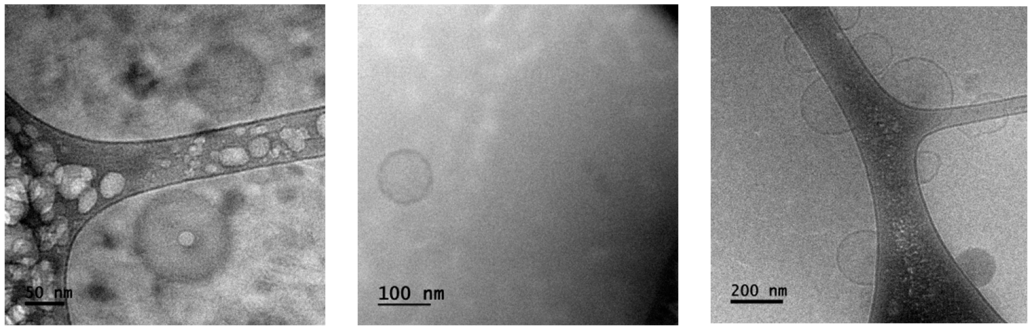

(**a**) (**b**) (**c**)

Figure 2. Representative TEM images: (**a**) agglomerated NDs encapsulated in liposomes; (**b**) typical view of pure liposomes; (**c**) typical evolution of liposomes with a trend of agglomeration.

These symmetry/asymmetry observations let us appreciate bigger (asymmetry) distributions and some clusters that could have significant dimensions; in contrast it seems that smaller distributions have better symmetry. These superficial properties in Figure 2a with respect to Figure 2b (roughness/smoothness and symmetry/asymmetry) will influence the optical response; however, further research concerning their influence in the release process (before and after crossing the laser diffusion barrier) needs to be analyzed widely. All nanoparticles move initially in a random individual motion as depicted in Figure 2b, and the liposome perfectly entraps a ND as observed in Figure 2a. When collisions occur between particles and self-assembled particles, a new group of nanovehicles forms immediately, thus, this new group continues a random motion within the fluids as a new cluster.

3.2. NDs Release

According to the theoretical models, mathematical formulations, and our experimental observations, the process by which NDs (drug product) leave liposomes (drug entrapper) could be described as follows: (1) Nanovehicles travel along a distance (l) to reach the TWM barrier with no intention to dissolve the drug product. In the absence of electromagnetic fields, most agglomerations of cells can act as natural barriers with low efficiency in the release process. (2) Immediate release—liposome starts slow interactions with photons coming from individual laser beams (ω_1–ω_2). (3) Agglomerations are formed (modified release), generating delayed and extended release of NDs due to strong interactions of photons with energy 2ω. (4) Delayed release is the process in which L + NDs are coming in delayed time and generating new and bigger auto-assembly formulations in the TWM border. (5) Extended release involves finite amounts of liposomes after strong interactions of photons. (6) Controlled release is driven by retarder $\lambda/2$ and the response of photodetectors PD1-2 increasing/decreasing as function of new assembly effects from pure NDs.

An extra stage (pulsatile release) is associated with the technical parameters from the laser source and their possible combinations. In vitro empirical and semi-empirical models and their stages have been accepted as important elements, in which under certain conditions they can be used to predict performance in in vivo or equivalence studies [30]; however, there is not a standard method yet, and each experiment and mathematical approach describes its own stages in accordance with its considerations [31]. Furthermore, functionalization of NPs suggests a preferential destruction of nanocarriers in cells, improving their ability to reduce bigger agglomerations in tissues and collateral damage in biological entities. At the same time, problems in their distribution can be remarkably controlled as compared to free drugs [32] or electromagnetic losses [33].

Optical mean behavior of each kind of set of samples (Samples A, B, and C) is plotted in Figure 3a; we observe the experimental absorbance at different excitation wavelengths. Standard 1 mm path length fluorescence cuvettes were used to run these absorbance measurements. From these experimental results we also observe a significance difference in the absorbance on two band ranges, the first one is in the range from 300 to 450 nm, and

the second one is in the range from 500 to 600 nm. This optical behavior is often explained by autofluorescence associated with medical conditions [34]. Some biological tests have proved that useful wavelengths in blood are in the range of 400 to 950 nm. Wavelengths longer than 600 nm are for bigger laser penetrations (>1 cm); shorter wavelengths are useful for smaller penetrations [35]. Within these regimes, the parameter (n) could be expected as $n < 1$ or $n > 1$. Outside of these regimes, the optical response is almost the same and it could be assumed that $n \approx 1$. We worked in the regime of 532 nm. Figure 3a shows that ethanol (Sample C) is a very poor absorber medium (lossless medium) while increasing the wavelength. Blood plasma under healthy and unhealthy (Samples A and B, respectively) conditions became equal absorptive after 800 nm. However, below the 700 nm region, differences were clearly observed.

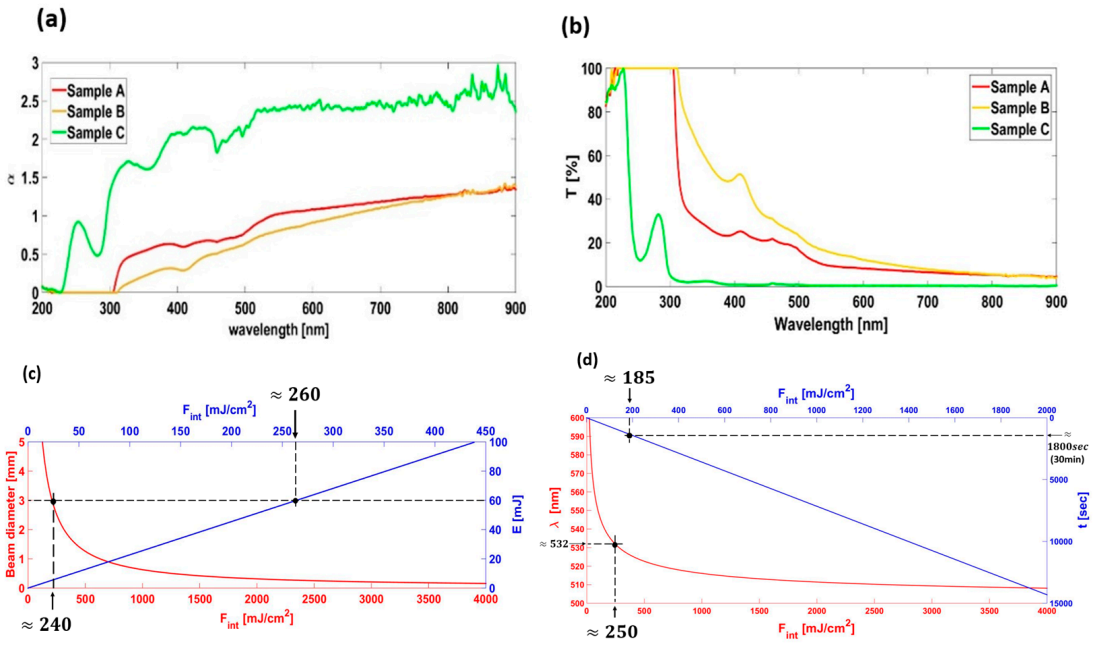

Figure 3. (**a**) Absorption coefficient in Samples A, B, and C; (**b**) transmittance properties; (**c**) integrated fluence as function of laser beam diameter and maximum pulse energy; (**d**) integrated fluence as function of wavelength (λ) and time exposure (t).

This optical behavior can also be related to the phenomenon of photon emission stimulated by the absorption of one (or more) photon(s) by surrounding cells that will return to their ground state. The rate of these kinds of interactions into the dissolution medium and under specific conditions (healthy/unhealthy) will influence the dissolution process of drugs. Aguiar et al. proposed the idea which holds that better observations of dissolution occur when the particles are in small sizes [36]. Wagner argued that pronounced effects of dissolutions occur for very well-shaped particles and the biological environment [37]. Probabilistic papers with mechanical systems and different fluids have been proposed as alternatives with an effective time release of near 15 min [38].

Each blood sample is proposed to be irradiated only once. The energy of the pump beam is the principal mechanism that is assumed to release NDs. Samples (S) were proposed to be left for 30 min (1800 s) at room temperature under the TWM configuration. At any point towards the propagation axis, the electronic oscillations of NDs radiate at angular frequencies 2ω in the direction of "k" (along the internal distance of the cuvette ϕ_{int} = 1.3 cm). The response evolution of PD1-2 will also be able to detect the release of NDs due to alterations of laser light travelling through each fluid. Physiological conditions are captured by the dynamical flow of nanovehicles traveling along the distance "l" of the cuvette. Direct current resistance modified by the electrical component of light is captured by the orthogonal axis of polarizers A1-2 and changes in PD1-2.

Technical adjustments associated with the optical path of each wave can be applied after being divided by the Beam Splitter (BS); if we did this, it would be possible to perform effective pulsatile damage. It is desirable to choose the best external parameters in order to have better control for drugs release. According to the laser device proposed in this experiment, we can obtain any of the combinations plotted in Figure 3c,d. From Equations (3) and (4) we obtain an expression for the theoretical integrated fluence in terms of the time exposure and the cross-sectional area of the laser spot. Figure 3c shows the influence in results of a beam diameter of 3 mm. We observed an integrated fluence near 240 mJ/cm^2, which will be the theoretical highest fluence generated in all three kinds of samples. This value of the integrated fluence increases non-linearly for smaller diameters of the beam. This tendency is congruent with similar experiments of ablation of different materials [39].

Furthermore, for this integrated fluence and the laser beam diameter, the theoretical input energy is 60 mJ per pulse. Considering 60 mJ per pulse, the total integrated fluence after 30 min will be near 260 mJ/cm^2. Experimental analyses considering just laser devices arrangement in blood plasma have demonstrated coagulation if the exposure is intense and short, whereas a laser exposure of insufficient intensity per pulse may nevertheless cause deep destruction of cells. Furthermore, damage results of a short exposure of short pulses at high intensity may be like those of long exposure at low intensity [40].

On the other hand, the damage energy of laser pulses as a function of time exposure is shown in Figure 3d. Exposures of 30 min (1800 s) have a theoretical integrated fluence of 185 mJ/cm^2 in the three sets of samples. In this figure, we also observe a correlation between the integrated fluence and wavelength. If λ is increasing, a non-linear behavior is generated and there is a sudden increment in the integrated fluence and bigger damage as we discussed before. This non-linear response was experimentally expected as a result of the observations in Samples A, B and C, plotted in the experimental group of results from Figure 3a. In this research, a wavelength of 532 nm corresponds to a 250 mJ/cm^2 theoretical integrated fluence.

Comparing the absorbance, α, plotted in Figure 3a, we can say that the release of NDs will be faster in the group of Samples A due to higher absorbance, and then higher temperature concentration and less laser energy necessary to release. In contrast, in the set of Samples B a higher laser energy is necessary to warm the fluid which means a lower absorption coefficient, lower laser efficiency, and long exposure. This behavior can be explained due to osmotic stress [41]. As a result of stresses relaxation and swelling, new mechanical properties of agglomerations can contribute to increase the release [42]. This mechanism can help to clarify the slow/high ablation temperatures at each set of samples [43]. Furthermore, these mechanical properties followed by the entrance of transparent particles/cells from fluids within nanovehicles help with a decrease in turbidity [44]. Opposite to this idea, when nanovehicles are subjected to outflow (hypertonic) atmospheres, the liposomal membrane becomes less permeable for drug liberation, resulting in an increment in turbidity [45,46]. Furthermore, big agglomerations are susceptible to bigger osmotic stress and stopped flow light scattering coefficients due to size changes [47]. These release mechanisms can be optically associated in terms of the refractive index (n) [44] described in the mathematical models in the previous section. However, as a result of the small size, experimental methods exhibit difficulties in directly observing the mechanical response with high accuracy; instead, optical experiments can be tracked [48].

3.3. Nanovehicles Diffusion

Nanovehicles will diffuse with a coefficient (D) through the distance (l), which represents the pipe length with blood plasma. In order to observe these effects, with the help of the spectrometer described before, we subjected samples of human blood plasma and ethanol to different wavelength doses to determine the optical parameters needed in the mathematical equations described in previous sections. The expected behavior associated with this idea is plotted in Figure 4. Experimental changes can be quantified by

the response of PD1-2, in which we evaluated the time required to reach, at least, a 50% increase/decrease in turbidity of each set of samples and as function of time (1800 s). Early works show that nanovehicles respond to these changes in turbidity after the equilibrium due to osmotic stresses which altered their mechanical properties, such as agglomerated area and the elasticity associated with the partial or total release of the entrapped cargo [49].

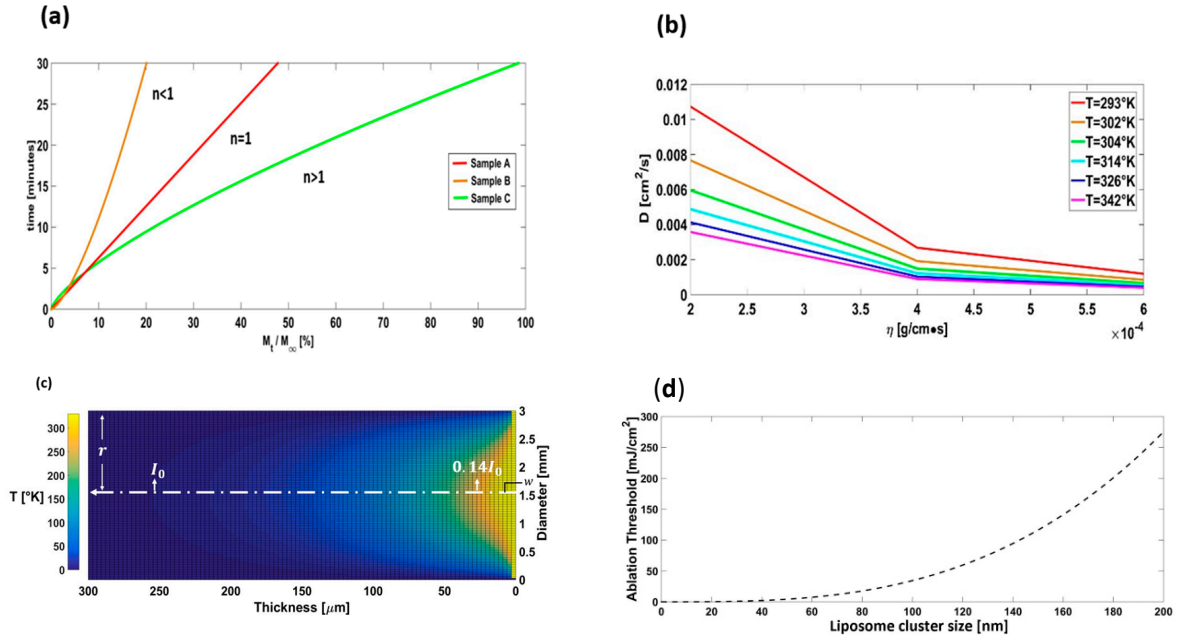

Figure 4. (**a**) Amount of nanovehicles accumulated; (**b**) diffusion coefficient upon irradiation as a function of viscosity of the samples for different temperatures; (**c**) temperature distribution at t = 30 min; (**d**) ablation threshold as a function of cluster size.

This is one of the bases of using liposomes as carriers of NDs, in which we propose to enhance the emission of biofluids after the release of NDs due to changes in mechanical and optical properties caused by the action of external laser pulses. With this in mind, we propose to establish a correlation between ablation/release mechanisms by quantifying the response of PD1-2 as a function of time. Some findings suggest that high levels of cells in plasma (healthy conditions) will initially saturate the surface of liposomes by a high density "corona" [50]; however, proteins at low concentrations (unhealthy conditions) may disassociate rapidly [51]. These kinds of effects are implicit in our results regarding particle diffusion labels and the interactions of probe/pump beams at the diffusion border (see Figures 3a and 4d).

The average experimental transmittance spectra in relation to wavelength are shown in Figure 3b. We observe different strong bands in all three nanofluids in the 250–600 nm range where the fluids have different response each other and no variations are observed from 700 nm; a future alternative to face this limitation could be the use of more accurate equipment, different numerical theories, and nanovehicles with different plasmon response. According to these figures, the useful amount of NDs (therapeutic agent) that cross the diffusion border is influenced by two factors in the TWM. One is the diffusion parameter plotted in Figure 4b as function of the fluids and nanovehicles properties described in Equation (5) (k). The second concerns on the experimental parameters measured with the evolution of the response of photodetectors PD1-2 and the evolution of temperatures within the sample (k'). At nearest values of $k \approx k'$, the increment in concentration, $\frac{M_t}{M_\infty}$, should be constant, giving the result that n tends to be equal (or close) to 1. This response has been generally known as zero-order transport kinetic or non-Fickian diffusion [28]. The other scenario concerns $n < 1$, this expression concerns a reduced diffusion gradient over time in which NDs have not been released and the optical response of the samples is not

enough to travel along the bulk fluid. Finally, in another possible scenario, the gradient is increasing periodically, resulting in a positive divergence from the linearity of mass transport rates. This performance is associated with $n > 1$ or $n >> 1$ and is generally called "superior case transporting" [28,52].

Figure 4a depicts the linear and non-linear response from the three kinds of samples and considering the experimental absorption coefficient (α) from Figure 3a at 532 nm. From the set of Samples B we observed the lowest gradient response of PD1-2 case in which $\frac{M_t}{M_\infty} \approx 14\%$ and assuming $n < 1$. The set of Samples A in Figure 4a depicts the zero-order transport in which the photodetector change was $\frac{M_t}{M_\infty} \approx 25\%$, and from Figure 3a we assumed $n \approx 1$ and, finally, the last scenario was assumed with $\frac{M_t}{M_\infty} \approx 50\%$ and $n > 1$ from Figure 3a (super case transport) in which the optical properties of NDs suggest an extra contribution in the optical properties due to agglomerations.

The evolution of heat distribution in the "super case" transportation was considered as well from the minimum and maximum temperatures developed in 30 min of time exposure and with Equation (7). In this case, we used the effect of the probe beam (ω_1). In Figure 4c this evolution is plotted with a Gaussian profile. The magnitude of the probe beam becomes weak transversely with a bell-shaped profile, which is symmetrical to the central axis depicted with a white dashed line with dots. In this case, the distance (r) passes through an imaginary circular aperture in the transverse plane of the spot beam (3 mm) and along its axis propagation. The distance, r, measured from the central axis, is then 1.5 mm with propagation to "k" direction ($k \approx 250$ μm). We can also observe that "r" represents the distance at which the photodamage of the beam drops from its maximum value.

Most of the photodamage of the beam resides within an imaginary cylinder of radius, w, where $w = \sqrt{(\lambda L)/(2\pi)}$, and L represents the distance of the spreading of the Gaussian beam (L = 1.3 cm). Most of the energy of the beam resides within this imaginary cylinder, of which the effective irradiance is described in Equation (1). According to these experimental results, the internal minimum radius of the probe beam is $w = 331.7^{-3}$ mm. At $r = w$ the beam effective irradiance is near 14% I_0 [25]. It means that only 14% of the theoretical value, 250 mJ/cm^2, will be effective to produce damage. However, absorption and transmittance experiments for simple view transparent fluids have reported absorptions near 9.16% and 13% [53,54].

Theoretical values for the ablation threshold (250 mJ/cm^2) predicted in Section 3.2 concerning technical parameters of the laser are near the experimental ones depicted in Table 1. According to experimental results, the integrated fluence, in which a change in photodetectors PD1 and PD2 is expected, has values of 123 mJ/cm^2 for nanovehicles and 181 mJ/cm^2 for pure liposomes. We need to consider the mechanical response of each biofluid and the medical condition to reach the theoretical value of 250 mJ/cm^2. On the other hand, the ablation time and the integrated fluence to release NDs can give practical and experimental information on the effective time in which a drug can be deposited into the plasma to produce therapeutic tasks. This process is best described in Figure 4d, in which non-linear response increases until the photon number of laser pulses begins to significantly deplete the population of liposomes from the upper level and NDs begin to release.

Table 1. Summary of optical and release properties of laser pulses in biological materials.

Material	Fluence [mJ/cm^2]	I_2 [MW/cm^2]	T [°C]
Liposome-encapsulated nanodiamonds (ND size 4–15 nm)	123 ± 30% (experiment) 250 (numerical)	39.79 (numerical)	51.85 (numerical) 50–70 [55]
Pure liposome	181 ± 30% (experiment)	58.56 (numerical) 0–300 [56]	40–50 [57]
Pure blood plasma	4000–5000 [58]	—-	80–100 [59]
Pure NDs	1,000,000 [60]	—-	—-

Conversion transitions during heat propagation describe the liposomes' population inversion that crosses the TWM barrier. When the population of liposomes reach the bottom of the cuvette, the pumping flux exceeds the calibrated parameters in PD1 due to stimulated emissions of NDs and the cycle begins again during the diffusion and release of L + NDs. Multicolor photoluminescent response after release can be excited at specific wavelengths (typically in the infrared regions) and better quantified spectroscopically [61].

The effect of corona formation behavior of the as-prepared nanovehicles in cells of plasma is expected considering Equation (7). We can assume this considering that viscosity increases in the cells in respect to the fluid where they are contained and then the diffusion coefficient decreases surrounding the cells to present the claimed corona effect.

Another principal parameter that we considered in the mechanical response is the total number of agglomerated NPs per area (D), the average diameter (d), and the amount of individual clusters we observed. In most of the typical nanofluids, the diameters of single particles begin from d = 5 to d = 50 nm; however, due to agglomeration effects, the particles become mostly considered from 70 to 200 nm [62]. Experimentally, it can be deduced that agglomerations can be generated by hundreds of elemental NPs. From our typical views of the aggregations observed in the TEM images, such as the one depicted in Figure 2a, we concluded that an aggregation cluster consists of 76 NPs comprising NDs with d = 17.3, which is in agreement within the limits of numerical models [63]. The temperature diffusion length (Figure 4c) promoted by multiple agglomerated microstructures in the "super case" transportation (best scenario in our experimental fluids) concerns 250 µm filled by 1.9×10^6 particles of clusters composed of NDs from d = 135 nm. Only 9.16 ± 14% will be the effective laser energy to produce the ablation threshold. The increment in inner force during liposome shrinkage increases the refractive index, elevating the light scattering. At the same time, small sizes in vehicles improve this effect in more turbid nanofluids (unhealthy conditions, $n < 1$) by diminishing the scattering ability.

In Figure 4b,c, the heat evolution is plotted as function of exposure (30 min). These analyses were obtained with help of Equation (7) and using the experimental results of optical and physical parameters. Boundary conditions were modelled in a one-side fixed cartesian coordinates system at the outer wall of SiO_2 with a temperature set to 0 °C. Inner-side limits concern the incident laser glass wall with L + ND over its surface. Changes in colors (yellow–orange) in Figure 4c represent the phase transitions (solid–liquid). In all of these numerical analysis, we considered a thickness z = 1.3 cm. According to our TEM observations, the average diameter of liposomes was near 200 nm, and the following parameters were obtained: R = 0.5, γ = 6.823, I_0 = 181 mJ/cm^2, and α = 0.6. We inferred that the temperature needed to start ablation of liposomes was ~30 °C (~300 °K). Our results agree with similar results of other experiments [64].

With similar analysis, we obtained the distribution of heat in NDs with 15 nm in diameter, reaching an outer radiation diameter of about 2100 microns, although the significant radiation is in the order of 500 microns. After 30 min of exposure, NDs will reach a temperature near 77 °C (350 °K). These numerical results were obtained as follows: $R = 0.5$, $\gamma = 0.829$, $I_0 = 123$ mJ/cm^2, and $\alpha = 0.5$. We also performed the heat distribution in the blood plasma under healthy conditions (Samples A). The optical, physical, and theoretical parameters considered were $R = 0.6$, $\gamma = 0.00418$, $I_0 = 250$ mJ/cm^2, and $\alpha = 1.2$. Finally, the mean heat distribution of the blood plasma of patients with diabetes mellitus, i.e., unhealthy conditions, were evaluated with the following parameters: $R = 0.8$, $\gamma = 0.00418$, $I_0 = 250$ mJ/cm^2, and $\alpha = 0.7$.

Spontaneous damage and cell fragmentation in blood has been revealed when heat propagation exceeds 50 °C (323 °K) after 30 min. Choi et al. found that blood plasma of humans treated at 50 °C during 5 min did not show evidence of permanent damage [65]. Plasmatic coagulations at temperatures of 55 °C (328 °K) and above induce an increase in cell fragmentation after 30 min of exposure. In this research, it is proposed to monitor the quick response with the help of photodetectors (PD1-2) before 32 °C (305 °K) and $t < 15$ min, which is lower than the irreversible injury. The increment in PD1-2 response is due to nanovehicles reaching a thermal equilibrium, NDs becoming immobile at the bottom of the tube, and therefore increasing their agglomeration size.

Knowing the diffusion level parameters, we can know the effective drug that has settled down with minimum absorption of molecules of the fluid. After 15 min, near 47 °C (320 °K), the damage temperature begins indicating plasmatic coagulation. This is accompanied by an increment in the magnitudes of PD1-2, suggesting that the PD1-2 starts receiving a bigger response and the release of NDs is taking place with an increment in heat to produce irreversible damage. The analysis of physicochemical properties of NPs agglomerations, between 5 and 200 nm, is important with this kind of aqueous media [66]. Further investigations on the development of sensing and release mechanisms of different hybrid biosensors within fluids are needed considering their luminescence properties and their sensitivity with help of the plasmonic response [67–69].

We highlight that optical methods present attractive advantages over other techniques as they allow us to monitor faster signals with a more efficient performance. Just to compare with a clear example, comparative dialysis methods can be effective, but they take time and different material resources, such as high-performance liquid chromatography (HPLC) systems, to quantify data.

Furthermore, the contact between nanovehicles and laser pulses can be increased by exploiting the gravitational and electromagnetic forces as well as the Brownian motion [70,71]. A future perspective is to analyze nanovehicles within insulin and blood plasma of diabetic/non-diabetic people to explain in further detail the agglomeration mechanism towards these fluids and with this kind of disease. In this sense, insulin resistance has spread to new areas, for which new angles are needed. Diabetes in its common form is known on the basis of raised plasma glucose levels, with a big variety of autoantibodies cells and other antigens [72] which increase the glucose levels that make the blood more viscous due to high blood glucose (blood sugar) in the body. As a result of high viscous values, we observe small values of the absorption coefficient, α; it implies that $n < 1$, so it could be predefined as an unhealthy condition of blood plasma. Pretty big values of α imply synthetic fluids in which $n >> 1$ (super case transport). Bigger values of α (healthy conditions) can be associated with $n \approx 1$. It was observed that with NPs loading, the absorption response can be increased up to nine times compared to pure fluids [73].

4. Conclusions

Pulsed-laser-induced structural changes in liposomes and NDs in blood plasma were evaluated using a TWM configuration. The adhesion of NDs and liposomes depends on changes in temperature due to laser beams and exposure time. Effects of agglomeration of clusters seem to be significant to the release of NDs by optical processes. The estimated

radiant exposure for the release of NDs onset was close to 123 mJ/cm^2; temperatures for the release are 27–37 °C; thermal degradation of liposomes induces a significant increase in light propagation through fluids. The optical response over the surface of NDs is related to the time- and temperature-dependent adhesion structure of nanovehicles. Significant increase in light response is expected after 15 min of radiant exposure. It seems that for bigger periods of laser irradiance (t > 15 min), there is a fall in thermal efficiency in the irradiated blood plasma. In shorter periods (t < 15 min), there is an increment in the absorbance, which is attributable to the presence of sugar agents. These types of studies could help to increase the understanding of the mechanisms of laser release of drugs in the future and avoid blood coagulation in quantitative and experimental ways. Further numerical correction coefficients are needed for predicting release onset.

Author Contributions: Writing—original draft, S.M.-B.; Conceptualization S.M.-B. and C.T.-T.; Writing—review and editing, S.M.-B., I.I.M.-D., J.D., A.F.-H., J.P.C.-L. and C.T.-T.; Investigation, S.M.-B., I.I.M.-D., J.D., A.F.-H., J.P.C.-L. and C.T.-T. All the authors contributed equally to the proposal and development of this research. The manuscript was written through the contribution of all authors. All authors have read and agreed to the published version of the manuscript.

Funding: This research was funded by Instituto Politécnico Nacional (SIP-2023), Universidad Politécnica del Valle de México, and Consejo Nacional de Ciencia y Tecnología (CONACyT).

Data Availability Statement: Data and materials are available upon reasonable request to C. Torres-Torres (ctorrest@ipn.mx).

Acknowledgments: The authors kindly acknowledge the Instituto Politécnico Nacional and Universidad Politécnica del Valle de México. The authors also acknowledge the facilities of "Centro Medico Nacional La Raza" for biological samples collection. The authors are also thankful to the Central Microscopy facilities of the Centro de Nanociencias y Micro y Nanotecnología del Instituto Politécnico Nacional.

Conflicts of Interest: The authors declare no conflict of interest.

References

1. Shengchun, Q.; Haibin, Y.; Dawei, R.; Shihai, K.; Guangtian, Z.; Dongmei, L.; Minghui, L. Magnetite Nanoparticles Prepared by Precipitation from Partially Reduced Ferric Chloride Aqueous Solutions Author links open overlay panel. *J. Colloid Interface Sci.* **1999**, *215*, 190–192. [CrossRef]
2. Widder, K.J.; Senyei, A.E.; Scarpelli, D.G. Magnetic microspheres: A model system for site specific drug delivery in vivo. *Proc. Soc. Exp. Biol. Med.* **1978**, *58*, 141–146. [CrossRef]
3. Hatch, G.P.; Stelter, R.E. Magnetic design considerations for devices and particles used for biological high-gradient magnetic separation (HGMS) systems. *J. Magn. Magn. Mater.* **2001**, *225*, 262–276. [CrossRef]
4. Bao, Z.; Liu, X.; Liu, Y.; Liu, H.; Zhao, K. Near-infrared light-responsive inorganic nanomaterials for photothermal therapy. *Asian J. Pharm. Sci.* **2016**, *11*, 349–364. [CrossRef]
5. Huang, X.; El-Sayed, M.A. Gold nanoparticles: Optical properties and implementations in cancer diagnosis and photothermal therapy. *J. Adv. Res.* **2010**, *1*, 13–28. [CrossRef]
6. Nilsson, A.M.; Lucassen, G.W.; Verkruysse, W.; Andersson-Engels, S.; van Gemert, M.J. Changes in optical properties of human whole blood in vitro due to slow heating. *Photochem. Photobiol.* **1997**, *65*, 366–373. [CrossRef] [PubMed]
7. Theis, J.H.; Ikeda, R.M.; Stobbe, D.; Ogata, C.; Lui, H.; Mason, D.T.; Lee, G. Effects of laser irradiation on human erythrocytes: Considerations concerning clinical laser angioplasty. *Clin. Cardiol.* **1983**, *6*, 396–398. [CrossRef]
8. Verkruysse, W.; Nilsson, A.M.; Milner, T.E.; Beek, J.F.; Lucassen, G.W.; van Gemert, M.J. Optical absorption of blood depends on temperature during a 0.5 ms laser pulse at 586 nm. *Photochem. Photobiol.* **1998**, *67*, 276–281. [CrossRef]
9. Pfefer, T.J.; Chan, K.F.; Hammer, D.X.; Welch, A.J. Pulsed holmium: YAG-induced thermal damage in albumen. In Proceedings of the Proceedings SPIE, Laser-Tissue Interaction IX, San Jose, CA, USA, 26–28 January 1998; Volume 3254, pp. 192–202. [CrossRef]
10. Ahmad, M.S.; Pandey, A.K.; Rahim, N.A. Effect of Nanodiamonds on the Optoelectronic Properties of TiO_2 Photoanode in Dye-Sensitized Solar Cell. *Arab. J. Sci. Eng.* **2018**, *43*, 3515–3519. [CrossRef]
11. Lisik, K.; Krokosz, A. Application of carbon nanoparticles in oncology and regenerative medicine. *Int. J. Mol. Sci.* **2021**, *22*, 8341. [CrossRef]
12. Kumar, V.B.; Perkas, N.; Porat, Z.E.; Gedanken, A. Solar-Light-Driven Photocatalytic Activity of Novel Sn@C-Dots-Modified TiO_2 Catalyst. *ChemistrySelect* **2017**, *2*, 6683–6688. [CrossRef]
13. Ngo, Y.-L.T.; Nguyen, P.L.; Jana, J.; Choi, W.M.; Chung, J.S.; Hur, S.H. Simple paper-based colorimetric and fluorescent glucose sensor using N-doped carbon dots and metal oxide hybrid structures. *Anal. Chim. Acta* **2021**, *1147*, 187–198. [CrossRef]

14. Kotta, S.; Aldawsari, H.M.; Badr-Eldin, S.M.; Alhakamy, N.A.; Shadab; Nair, A.B.; Deb, P.K. Exploring the Potential of Carbon Dots to Combat COVID-19. *Front. Mol. Biosci.* **2020**, *7*, 616575. [CrossRef] [PubMed]
15. Shenderova, O.A.; Gruen, D.M. Advances in synthesis and processing. In *Book Ultrananocrystalline Diamond: Synthesis, Properties, and Applications*, 2nd ed.; William Andrew Elsevier: New York, NY, USA, 2006; pp. 3–44.
16. Kubo, T.; Sugita, T.; Shimose, S.; Nitta, Y.; Ikuta, Y.; Murakami, T. Targeted systemic chemotherapy using magnetic liposomes with incorporated adriamycin for osteosarcoma in hamsters. *Int. J. Oncol.* **2001**, *18*, 121–126. [CrossRef] [PubMed]
17. Agrawal, U.; Sharma, R.; Gupta, M.; Vyas, S.P. Is nanotechnology a boon for oral drug delivery? *Drug Discov. Today* **2014**, *19*, 1530–1546. [CrossRef]
18. Sgorla, D.; Bunhak, É.J.; Cavalcanti, O.A.; Fonte, P.; Sarmento, B. Exploitation of lipid-polymeric matrices at nanoscale for drug delivery applications. *Expert Opin. Drug Deliv.* **2016**, *13*, 1301–1309. [CrossRef] [PubMed]
19. Gregoriadis, G.; Ryman, B.E. Liposomes as carriers of enzymes or drugs: A new approach to the treatment of storage diseases. *Biochem. J.* **1971**, *124*, 58P. [CrossRef]
20. Mayhew, E.; Papahadjopoulos, D.; Rustum, Y.M.; Dave, C. Inhibition of tumor cell growth in vitro and in vivo by 1-beta-D-arabinofuranosylcytosine entrapped within phospholipid vesicles. *Cancer Res.* **1976**, *36*, 4406–4411.
21. Laginha, K.M.; Verwoert, S.; Charrois, G.J.; Allen, T.M. Determination of doxorubicin levels in whole tumor and tumor nuclei in murine breast cancer tumors. *Clin. Cancer Res.* **2005**, *11*, 6944–6949. [CrossRef]
22. Johnston, M.J.; Semple, S.C.; Klimuk, S.K.; Edwards, K.; Eisenhardt, M.L.; Leng, E.C.; Karlsson, G.; Yanko, D.; Cullis, P.R. Therapeutically optimized rates of drug release can be achieved by varying the drug-to-lipid ratio in liposomal vincristine formulations. *Biochim. Biophys. Acta* **2006**, *1758*, 55–64. [CrossRef]
23. Bothun, G.D. Hydrophobic silver nanoparticles trapped in lipid bilayers: Size distribution, bilayer phase behavior, and optical properties. *J. Nanobiotechnol.* **2008**, *6*, 13. [CrossRef]
24. Douda, J.; González-Vargas, C.R.; Mota-Díaz, I.I.; Basiuk, E.V.; Hernández-Contreras, X.A.; Fuentes-García, J.A.; Bornacelli, J.; Torres-Torres, C. Photoluminescent properties of liposome-encapsulated amine-functionalized nanodiamonds. *Nano Express* **2020**, *1*, 030009. [CrossRef]
25. Eugene, H. Modern Optics: Lasers and Other Topics. In *Book Optics*, 5th ed.; Pearson, United States Edition: New York, NY, USA, 2016; pp. 625–627.
26. Raciukaitis, G.; Brikas, M.; Gecys, P.; Gedvilas, M. Accumulation effects in laser ablation of metals with high-repetition-rate lasers. In Proceedings of the SPIE, High-Power Laser Ablation VII, Taos, NM, USA, 20–24 April 2008; Volume 7005. [CrossRef]
27. Nelson, E. Chapter 4 Albert Einstein. In *Book Dynamical Theories of Brownian Motion*, 2nd ed.; Princeton University Press: Princeton, NJ, USA, 2020; pp. 13–17.
28. Jain, A.; Jain, S.K. In Vitro release model fitting of liposomes: An insight. *Chem. Phys. Lipids* **2016**, *201*, 28–40. [CrossRef]
29. Paula, S.; Volkov, A.G.; Van Hoek, A.N.; Haines, T.H.; Deamer, D.W. Permeation of protons, potassium ions, and small polar molecules through phospholipid bilayers as a function of membrane thickness. *Biophys. J.* **1996**, *70*, 339–348. [CrossRef] [PubMed]
30. Solomon, D.; Gupta, N.; Mulla, N.S.; Shukla, S.; Guerrero, Y.A.; Gupta, V. Role of in vitro release methods in liposomal formulation development: Challenges and reg-ulatory perspective. *AAPS J.* **2017**, *19*, 1669–1681. [CrossRef] [PubMed]
31. Nothnagel, L.; Wacker, M.G. How to measure release from nanosized carriers? *Eur. J. Pharm. Sci.* **2018**, *120*, 199–211. [CrossRef] [PubMed]
32. Morales-Bonilla, S.; Mota-Díaz, I.I.; Douda, J.; González-Vargas, C.R.; Villalpando, I.; Torres-Torres, C. Thermo-mechanical effects and photo-induced release of liposome-encapsulated nanodiamonds by polarization-resolved laser pulses. *Optik* **2021**, *245*, 167738. [CrossRef]
33. Torres-Torres, R. Extracting characteristic impedance in low-loss substrates. *Electron. Lett.* **2011**, *47*, 191. [CrossRef]
34. Mansfield, J.R.; Gossage, K.W.; Hoyt, C.C.; Levenson, R.M. Autofluorescence removal, multiplexing, and automated analysis methods for in-vivo fluorescence imaging. *J. Biomed. Opt.* **2005**, *10*, 41207. [CrossRef]
35. Farkas, J.P.; Hoopman, J.E.; Kenkel, J.M. Five Parameters You Must Understand to Master Control of Your Laser/Light-Based Devices. *Aesthet. Surg. J.* **2013**, *33*, 1059–1064. [CrossRef]
36. Aguiar, A.J.; Krc, J., Jr.; Kinkel, A.W.; Samyn, J.C. Effect of polymorphism on the absorption of chloramphenicol from chloramphenicol palmitate. *J. Pharm. Sci.* **1967**, *56*, 847–853. [CrossRef]
37. Wagner, J.G. Biopharmaceutics: Absorption aspects. *J. Pharm. Sci.* **1961**, *50*, 359–387. [CrossRef] [PubMed]
38. Bhakta, H.C.; Lin, J.M.; Grover, W.H. Measuring dissolution profiles of single controlled-release drug pellets. *Sci. Rep.* **2020**, *10*, 19734. [CrossRef]
39. Kautek, W.; Krüger, J. Femtosecond pulse laser ablation of metallic, semiconducting, ceramic, and biological materials. In Proceedings of the Laser Materials Processing: Industrial and Microelectronics Applications, Vienna, Austria, 7 September 1994.
40. Ye, H.; De, S. Thermal injury of skin and subcutaneous tissues: A review of experimental approaches and numerical models. *Burn. J. Int. Soc. Burn. Inj.* **2017**, *43*, 909–932. [CrossRef]
41. Abuin, E.; Lissi, E.; Ahumada, M. Diffusion of hydrogen peroxide across DPPC large unilamellar liposomes. *Chem. Phys. Lipids* **2012**, *165*, 656–661. [CrossRef] [PubMed]
42. Ahumada, M.; Calderón, C.; Leon, L.; Lissi, E. Rate of solute incorporation to liposomes evaluated from encapsulated enzymes activities. *Biophys. Rev.* **2014**, *6*, 161–167. [PubMed]

43. Ueno, M.; Yoshida, S.; Horikoshi, I. Characteristics of the membrane permeability of temperature-sensitive liposomes. *Bull. Chem. Soc. Jpn.* **1991**, *64*, 1588–1593.
44. White, G.; Pencer, J.; Nickel, B.G.; Wood, J.M.; Hallet, F.R. Optical changes in unilamellar vesicles experiencing osmotic stress. *Biophys. J.* **1996**, *71*, 2701–2715.
45. Fujiwara, K.; Yanagisawa, M. Generation of giant unilamellar liposomes containing biomacromolecules at physiological intracellular concentrations using hypertonic conditions. *ACS Synth. Biol.* **2014**, *3*, 870–874. [CrossRef]
46. Disalvo, E.A.; Campos, A.M.; Abuin, E.; Lissi, E. Surface changes induced by osmotic shrinkage on large unilamellar vesicles. *Chem. Phys. Lipids* **1996**, *84*, 35–45.
47. Sun, S.-T.; Milon, A.; Tanaka, T.; Ourisson, G.; Nakatani, Y. Osmotic swelling of unilamellar vesicles by the stopped-flow light scattering method. Elastic properties of vesicles. *Biochim. Biophys. Acta Biomembr.* **1986**, *860*, 525–530. [CrossRef]
48. Chen, P.Y.; Pearce, D.; Verkman, A.S. Membrane water and solute permeability deter-mined quantitatively by self-quenching of an entrapped fluorophore. *Biochemistry* **1988**, *27*, 5713–5718.
49. Ertel, A.; Marangoni, A.; Marsh, J.; Ross Hallett, F.; Wood, J. Mechanical properties of vesicles. 1. Coordinated analyses of osmotic swelling and lysis. *Biophys. J.* **1993**, *64*, 426–434.
50. Lynch, I.; Dawson, K.A.; Linse, S. Detecting cryptic epitopes created by nanoparticles. *Sci. STKE* **2006**, *2006*, pe14. [CrossRef] [PubMed]
51. Gray, J.J. The interaction of proteins with solid surfaces. *Curr. Opin. Struct. Biol.* **2004**, *14*, 11011–110115. [CrossRef]
52. Costa, P.; Sousa Lobo, J.M. Modeling and comparison of dissolution profiles. *Eur. J. Pharm. Sci.* **2001**, *13*, 123–133. [CrossRef] [PubMed]
53. Drotning, W.D. Optical properties of solar-absorbing oxide particles suspended in a molten salt heat transfer fluid. *Sol. Energy* **1978**, *20*, 313–319.
54. Otanicar, T.P.; Phelan, P.E.; Golden, J.S. Optical properties of liquids for direct ab-sorption solar thermal energy systems. *Sol. Energy* **2009**, *83*, 969–977. [CrossRef]
55. Grundfest, W.S.; Litvack, F.; Forrester, J.S.; Goldenberg, T.S.; Swan, H.J.; Morgenstern, L.; Fishbein, M.; McDermid, I.S.; Rider, D.M.; Pacala, T.J.; et al. Laser ablation of human atherosclerotic plaque without adjacent tissue injury. *J. Am. Coll. Cardiol.* **1985**, *5*, 929–933. [CrossRef]
56. Miranda, D.; Carter, K.; Luo, D.; Shao, S.; Geng, J.; Li, C.; Chitgupi, U.; Turowski, S.G.; Li, N.; Atilla-Gokcumen, G.E.; et al. Multifunctional Liposomes for Image-Guided Intratumoral Chemo-Phototherapy. *Adv. Healthc. Mater.* **2017**, *6*, 1700253. [CrossRef]
57. Rossmann, C.; McCrackin, M.A.; Armeson, K.E.; Haemmerich, D. Temperature sensitive liposomes combined with thermal ablation: Effects of duration and timing of heating in mathematical models and in vivo. *PLoS ONE* **2017**, *12*, e0179131. [CrossRef]
58. Black, J.F.; Wade, N.; Barton, J.K. Mechanistic comparison of blood undergoing laser photocoagulation at 532 and 1064 nm. *Laser Surg. Med.* **2005**, *36*, 155–165. [CrossRef]
59. Pfefer, T.J.; Choi, B.; Vargas, G.; McNally-Heintzelman, K.M.; Welch, A.J. Mechanisms of laser-induced thermal coagulation of whole blood in vitro. In Proceedings of the SPEI, Lasers in Surgery: Advanced Characterization, Therapeutics, and Systems IX, San Jose, CA, USA, 23–29 January 1999; Volume 3590. [CrossRef]
60. Pichot, V.; Muller, O.; Seve, A.; Yvon, A.; Merlat, L.; Spitzer, D. Optical properties of functionalized nanodiamonds. *Sci. Rep.* **2017**, *7*, 14086. [CrossRef]
61. Jiang, K.; Sun, S.; Zhang, L.; Lu, Y.; Wu, A.; Cai, C.; Lin, H. Red, green, and blue luminescence by carbon dots: Full-color emission tuning and multicolor cellular imaging. *Angew. Chem. Int. Ed. Engl.* **2015**, *54*, 5360–5363. [CrossRef] [PubMed]
62. Taylor, R.A.; Phelan, P.E.; Otanicar, T.P.; Adrian, R.; Prasher, R. Nanofluid optical property characterization: Towards efficient direct absorption solar collectors. *Nanoscale Res. Lett.* **2011**, *6*, 225. [CrossRef]
63. Tesfai, W.; Singh, P.K.; Masharqa, S.J.S.; Souier, T.; Chiesa, M.; Shatlla, Y. Investigating the effect of suspensions nanostructure on the thermophysical properties of nanofluids. *J. Appl. Phys.* **2012**, *112*, 114315. [CrossRef]
64. Frich, L.; Bjørnerud, A.; Fossheim, S.; Tillung, T.; Gladhaug, I. Experimental application of thermosensitive paramagnetic liposomes for monitoring magnetic resonance imaging guided thermal ablation. *Magn. Reson. Med.* **2004**, *52*, 1302–1309. [CrossRef] [PubMed]
65. Choi, J.W.; Pai, S.H. Changes in hematologic parameters induced by thermal treatment of human blood. *Ann. Clin. Lab. Sci.* **2002**, *32*, 393–398. [PubMed]
66. Kreuter, J. Drug targeting with nanoparticles. *Eur. J. Drug Metab. Pharmacokinet.* **1994**, *19*, 253–256. [CrossRef]
67. Ma, Q.M.; Zhang, M.; Xu, X.H.; Meng, K.; Yao, C.; Zhao, Y.F.; Sun, J.; Du, Y.P.; Yang, D.Y. Multiresponsive Supramolecular Luminescent Hydrogels Based on a Nucleoside/Lanthanide Complex. *ACS Appl. Mater. Interfaces* **2019**, *11*, 47404–47412. [CrossRef] [PubMed]
68. Morales-Bonilla, S.; Torres-Torres, C.; Trejo-Valdez, M.; Torres-Torres, D.; Urriolagoitia-Calderón, G. Mechano-optical transmittance and third order nonlinear optical properties exhibited by Au nanoparticles. *Optik* **2015**, *126*, 4093–4097. [CrossRef]
69. Lin, Z.Y.; Qu, Z.B.; Chen, Z.H.; Han, X.Y.; Deng, L.X.; Luo, Q.Y.; Jin, Z.W.; Shi, G.Y.; Zhang, M. The Marriage of Protein and Lanthanide: Unveiling a Time-Resolved Fluorescence Sensor Array Regulated by pH toward High-Throughput Assay of Metal Ions in Biofluids. *Anal. Chem.* **2019**, *91*, 11170. [CrossRef] [PubMed]

70. Plank, C.; Schillinger, U.; Scherer, F.; Bergemann, C.; Rémy, J.S.; Krötz, F.; Anton, M.; Lausier, J.; Rosenecker, J. The magnetofection method: Using magnetic force to enhance gene delivery. *Biol. Chem.* **2003**, *384*, 737–747. [CrossRef] [PubMed]
71. Morales-Bonilla, S.; Martines-Arano, H.; Torres-Torres, D.; Ochoa-Ortega, G.; Carrillo-Delgado, C.; Trejo-Valdez, M.; Torres-Torres, C. Dynamic and plasmonic response exhibited by Au nanoparticles suspended in blood plasma and cerebrospinal fluids. *J. Mol. Liquids* **2019**, *281*, 1–8. [CrossRef]
72. Zimmet, P.Z. The pathogenesis and prevention of diabetes in adults. Genes, autoimmunity, and demography. *Diabetes Care* **1995**, *18*, 1050–1064. [CrossRef]
73. Tyagi, H.; Phelan, P.; Prasher, R. Predicted efficiency of a low-temperature nanofluid-based direct absorption solar collector. *ASME J. Sol. Energy Eng.* **2009**, *131*, 041004. [CrossRef]